

Memory-function approach to the normal-state optical properties of the Bechgaard salt (TMTSF)₂PF₆

Ivan Kupčić*

Department of Physics, Faculty of Science, P.O.B. 331, HR-10 002 Zagreb, Croatia

The gauge invariant, two-component optical conductivity model, with a correlation gap structure related to the umklapp scattering processes, is applied to the quasi-one-dimensional electronic systems and compared to the recent measurements on the Bechgaard salt (TMTSF)₂PF₆. The optical response of both the insulating and metallic state is found for the half-filled conduction band, depending on the ratio between the correlation energy scale $2\Delta_2^0$ and the transfer integral in the direction perpendicular to the conducting chains, $t_{b'}$. The estimated value $2\Delta_2^0/t_{b'}$ agrees reasonably well with the previous experimental and theoretical conclusions. Parallel to the chains the thermally activated conduction electrons in the insulating state are found to exhibit an universal behaviour, accounting for the observed single-particle optical conductivity of the ordered ground state of charge-density-wave systems. The band parameters and the related damping energies suitable to the normal metallic state of (TMTSF)₂PF₆ are estimated from the measured spectra. Not only the spectral weights but also the damping energies clearly indicate an opening of the correlation gap in the charge excitation spectrum.

PACS numbers: 78.20.Bh; 75.30.Fv

Keywords: Optical properties; SDW materials; Umklapp processes; Confinement-deconfinement

I. INTRODUCTION

The electrodynamics of quasi-one-dimensional (Q1D) and two-dimensional (2D) electronic systems has been the subject of intensive experimental investigation [1, 2, 3, 4, 5, 6, 7, 8, 9, 10], in part because various correlation and dimerization gaps in the charge excitation spectrum are observed recently in the measurements conducted on several high quality single crystals. Strong evidence for an unusual metallic state in the Bechgaard salts (TMTSF)₂X, where $X = \text{PF}_6$, AsF_6 or ClO_4 , has been found not only at temperatures close to the critical spin-density-wave (SDW) temperature, T_{SDW} , but also at temperatures well above T_{SDW} [4].

The anomalies observed in (TMTSF)₂PF₆ in the latter temperature range are the focus of the present analysis (the data measured at $T \approx 20$ K and $T \approx 100$ K [3, 4, 5] will be considered here as the typical representatives of the $T \approx T_{\text{SDW}}$ and $T \gg T_{\text{SDW}}$ spectra). The most pronounced anomalous features characterizing the spectra measured for the electromagnetic fields polarized in the highly conducting direction are as follows. (i) The spectral weight of the zero-frequency peak is almost independent of temperature, with the related effective number of conducting electrons $n_{\text{intra},a}^{\text{eff}} \approx n/100$ indicating the deconfined (metallic) state of the electronic system ($n = 1/V_0$ is the hole concentration, with V_0 being the primitive cell volume). (ii) There is a pronounced deviation of the zero-frequency conductivity from a simple Drude behaviour which points at substantial frequency correc-

tions in the “intraband” damping energy $\hbar\Gamma_{\text{intra}}$. (iii) The maximum in the mid-infrared (MIR) optical conductivity shifts from $\omega_{\text{peak}}/(2\pi c) = 250 \text{ cm}^{-1}$ at $T = 20$ K to $\omega_{\text{peak}}/(2\pi c) = 800 \text{ cm}^{-1}$ at $T = 300$ K, which is approximately the temperature dependence expected for the “interband” damping energy $\hbar\Gamma_{\text{inter}}$. (iv) This peak broadens with temperature exhibiting both a strong sub-gap conductivity (with $\hbar\Gamma_{\text{inter}} \approx 30 \text{ meV}$ at room temperatures, estimated in Ref. [11]) and a non-universal (temperature-dependent) power-law behaviour of the optical conductivity in the frequency range $\omega \gg \omega_{\text{peak}}$.

In order to discuss these anomalies and the existing theories describing the electrodynamics of the strongly correlated strictly 1D or Q1D systems [11, 12, 13, 14, 15, 16, 17, 18, 19, 20], we will consider here a simple, single-particle model of the conduction electrons in the presence of both two gaps and external electromagnetic fields. It is already shown that such a model gives rise the exact solution of the site-energy dimerization problem (for example, the anion ordering in (TMTSF)₂ClO₄) [21], as well as a good approximation for the weak bond-energy dimerization (and the related single-particle properties of the crystals with the charge-density-wave (CDW) ground state) [19]. Here we will show that this model also provides a reasonable description of the correlation effects related to the umklapp scattering processes. Unlike the exact treatment of the umklapp in the strictly 1D approaches based on the bosonization procedure [15, 18], suitable to temperatures close to T_{SDW} , the present model describes the electrodynamics of the interacting electronic system at $T \gg T_{\text{SDW}}$ in terms of the effective fermions, and, consequently, is the subject of easy comparison with similar fermionic analyses concerned with the room temperature electrodynamic features [11, 17] or

*E-mail address: kupcic@phy.hr (I. Kupčić)

with other (anomalous) properties of the normal metallic state of these salts [1, 22, 23, 24].

The article is organized as follows. In Section 2 and Appendix A we present the two-component optical conductivity for the Q1D electronic system with the dimerization/correlation gap in the single-particle excitation spectrum, which is a simple extension of the memory-function formalism [15, 25, 26, 27]. The confinement of conduction electrons to the highly conducting chains is discussed in Section 3, by considering the spectral weights of the zero-frequency and MIR optical conductivity as a function of the crossover parameter, i.e. of the ratio between the gap magnitude and the transfer integral in the direction perpendicular to the chains. The interplay among the small parameters of the two-component optical model is illustrated then for the insulating and metallic state of the half-filled band. The results are compared to the experimental spectra of (TMTSF)₂PF₆. The concluding remarks are given in the last section.

II. THEORETICAL MODEL

In this section, the memory-function theory will be applied to determine the response of a simple Q1D metallic system to the external electromagnetic fields. The electrons are assumed to be affected by two single-particle perturbations $\Delta_m(\mathbf{k})$ with the commensurate wave vectors $\mathbf{Q}_m = (2\pi/(ma), 0)$, $m = 1$ and 2 (where $\mathbf{Q}_2 \approx 2\mathbf{k}_F$). $\mathbf{a} = a\hat{x}$ and $\mathbf{b}' = b'\hat{y}$ are the primitive vectors of the rectangular Bravais lattice, and the x -axis is along the highly conducting direction. For the Bechgaard salts, $\Delta_1(\mathbf{k})$ is the potential related to the bond-energy dimerization along the x -axis, and $\Delta_2(\mathbf{k})$ is an effective perturbation which will model the opening of the pseudogap in the charge excitation spectrum caused by the umklapp scattering processes. However, it must be noted that the present consideration will be restricted to temperatures well above T_{SDW} ($T_{\text{SDW}} \approx 12$ K in (TMTSF)₂PF₆ [4]), and, consequently, the nesting features of the Fermi surface responsible for the SDW instability of the electronic system will be disregarded.

In order to make the generalization of the memory-function approach more straightforward, the analysis is divided into three steps. For the crystallographic data characterizing the Bechgaard salts, the direct effects of $\Delta_1(\mathbf{k})$ on the current-current correlation function are found to be negligible [11]. This issue is briefly reconsidered in Section 2.1. In Section 2.2 the corresponding indirect effects are parametrized in terms of the umklapp interaction $g_{1/2}$ [28], and treated by means of the mean-field approximation. The current-current correlation functions are determined then for the case of low impurity concentration. Finally, after ensuring that the resulting optical conductivity obeys the causality properties, the residual scattering processes are taken into account in Section 2.3.

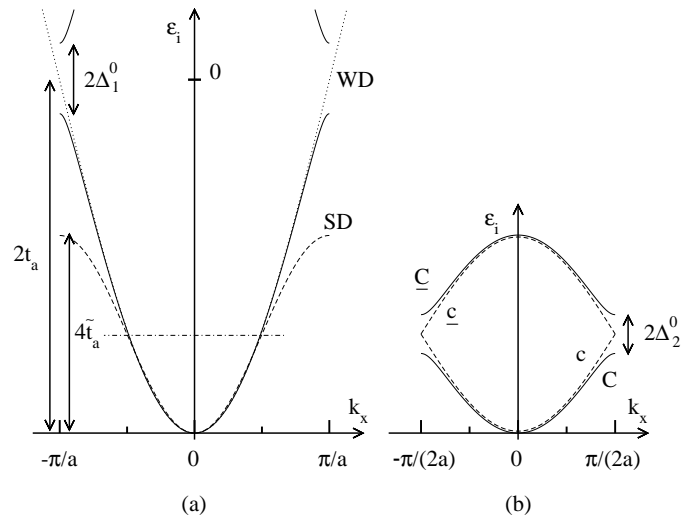


FIG. 1: The hole dispersions $\varepsilon_i(k_x, \pi/(2b'))$ (solid lines) as a function of the perturbations $\Delta_1(\mathbf{k})$ (a) and $\Delta_2(\mathbf{k})$ (b). The $\Delta_1(\mathbf{k}) \neq 0$ dispersion is contrasted to the weak-dimerization (WD) and strong-dimerization (SD) dispersions defined in the text. The dot-dashed line is the Fermi level in the quarter-filled $\Delta_1(\mathbf{k}) = 0$ band, and $\varepsilon_F = \varepsilon_0(\pi/(2a), \pi/(2b')) - \varepsilon_0(0, \pi/(2b'))$ is the related Fermi energy. The dispersions of the $\Delta_2(\mathbf{k}) = 0$ and $\Delta_2(\mathbf{k}) \neq 0$ SD models are shown in the reduced zone representation; c , \underline{c} and C , \underline{C} are the corresponding band indices.

A. Bond-energy dimerization

The bond-energy dimerization along the highly conducting chain axis occurs in all Bechgaard salts, and is usually described in terms of the dimensionless parameter $\alpha = (a_1 - a_2)/a$, with a_1 and a_2 being nearest-neighbor distances and $a = a_1 + a_2$. In (TMTSF)₂PF₆ the characteristics of the triclinic Bravais lattice are found to be $a_1 - a_2 = 0.03$ Å, $a = 7.297$ Å, $b' = b \sin \gamma = 7.291$ Å and $V_0 = \mathbf{a} \cdot (\mathbf{b} \times \mathbf{c}) = 714.3$ Å³ [1, 29].

In these compounds the conduction electrons are usually described using the quarter-filled hole band $\varepsilon_0(\mathbf{k}) = -2t_a \cos \frac{1}{2}\mathbf{k} \cdot \mathbf{a} - 2t_{b'} \cos \mathbf{k} \cdot \mathbf{b}'$, with the perturbation $\Delta_1(\mathbf{k}) = ig\alpha \sin \frac{1}{2}\mathbf{k} \cdot \mathbf{a}$. Here t_a and $t_{b'}$ are the bond-energies for $\alpha = 0$, and g is the related electron-phonon coupling. After diagonalization the lower band becomes half-filled, with the dispersion $\varepsilon(\mathbf{k}) = (1/2)[\varepsilon_0(\mathbf{k}) + \varepsilon_0(\mathbf{k} \pm \mathbf{Q}_1)] - \sqrt{(1/4)[\varepsilon_0(\mathbf{k}) - \varepsilon_0(\mathbf{k} \pm \mathbf{Q}_1)]^2 + |\Delta_1(\mathbf{k})|^2}$, as illustrated in Fig. 1(a).

The spectral weight of the interband optical excitations relative to the total spectral weight is given approximately by $[\Delta_1^0/|\varepsilon(\mathbf{k}_F)|]^2$, with $\Delta_1^0 = g\alpha$ representing the magnitude of the dimerization potential and $E_{g1} \approx |2\varepsilon(\mathbf{k}_F)|$ is the related threshold energy (see the difference between the total and intraband spectral weights for the case $\Delta(\mathbf{k}) \rightarrow \Delta_1(\mathbf{k})$ in Eqs. (28), (21), (29) and (A6)). At least in (TMTSF)₂PF₆ this ratio is negligible [11]. Therefore, the direct effects of $\Delta_1(\mathbf{k})$ on the optical conductivity will not affect the forthcoming analysis

and we can write the bare hole dispersion in the form $\varepsilon(\mathbf{k}) \approx \varepsilon_0(\mathbf{k})$ (hereafter, this limit is referred to as the weak-dimerization (WD) limit, see Fig. 1(a)). Consequently, the quantitative analysis of the spectral weights in Sec. 2.3 will employ the WD dispersion. On the other hand, for the qualitative consideration of the low-frequency spectra, the strong-dimerization (SD) dispersion is more adequate due to simple symmetry properties of both $\varepsilon(\mathbf{k})$ and the related current and Raman vertex functions.

B. Umklapp scattering processes in the mean-field approximation

From the work of Emery et al. [28] it is known that the electrodynamic features of the Bechgaard salts are affected by the bond-energy dimerization dominantly through the umklapp interaction $g_{1/2} \propto U\Delta_1^0/\varepsilon_F$. Their conclusions have been supported by the systematic investigation of the optical conductivity in the MIR part of the spectra [5]. It has been established that, as α shifts to higher values, the energy $E_{\text{peak}} = \hbar\omega_{\text{peak}}$ becomes larger going from $E_{\text{peak}} \approx 25$ meV in (TMTSF)₂PF₆ ($\alpha \approx 0.004$ [28]) to $E_{\text{peak}} \approx 200$ meV in (TMTTF)₂PF₆ ($\alpha \approx 0.014$). Additional evidence for the crucial role of these scattering processes was given by Favand and Mila [17], considering the MIR optical features of the dimerized 1D Hubbard model. They have found that the dimerization potential, together with the strong Hubbard interaction U , results in a renormalized threshold energy $E_{g2} \sim 2\Delta_1^0$, in addition to the bare threshold energy E_{g1} ($E_{g2} \ll E_{g1}$).

In order to study the influence of these processes on the electrodynamics of the conduction electrons described by the (WD or SD) hole dispersion $\varepsilon(\mathbf{k})$ at $T \gg T_{\text{SDW}}$, we adopt now the mean-field approximation, with the effective perturbation $\Delta_2(\mathbf{k}) \propto g_{1/2}$.

1. Model Hamiltonian

As illustrated in Fig. 1(b), the electrons are shown in the zone representation $|k_x| < \pi/(2a)$, $|k_y| < \pi/b'$ (for simplicity, the 2D Brillouin zone of (TMTSF)₂PF₆ is approximated by the rectangular zone). The band indices of $\Delta_2^0 = 0$ and $\Delta_2^0 \neq 0$ will be denoted by $l \in \{c, \underline{c}\}$ and $\bar{L} \in \{C, \underline{C}\}$, respectively. The $\varepsilon_l(\mathbf{k})$ and $E_L(\mathbf{k})$ are the related hole dispersions (obviously, $\varepsilon_c(\mathbf{k}) = \varepsilon(\mathbf{k})$ and $\varepsilon_{\underline{c}}(\mathbf{k}) = \varepsilon(\mathbf{k} \pm \mathbf{Q}_2)$). For the sake of generality, the index $m = 2$ (in $\Delta_2(\mathbf{k})$, \mathbf{Q}_2 and $E_{g2} = E_{\underline{C}}(\mathbf{k}_F) - E_C(\mathbf{k}_F)$; E_{g2} is the MIR threshold energy) will be omitted and an arbitrary filling of the conduction band will be assumed. The final results (Section 3) will be given for $\mathbf{Q} \rightarrow \mathbf{Q}_2 \approx 2\mathbf{k}_F$, with the index $m = 2$ explicitly written [30].

The total Hamiltonian reads as

$$H = H_0 + H'_1 + H'_2 + H^{\text{ext}}. \quad (1)$$

H_0 is the bare Hamiltonian. H'_1 represents the single-particle scattering processes (due to impurities, phonons, CDW or SDW fluctuations) and H^{ext} is the coupling Hamiltonian which couples the electromagnetic fields to the current and Raman density fluctuations. In the memory-function approach at temperatures well above T_{SDW} the residual two-particle scattering processes, represented here by H'_2 , play usually the marginal role and therefore will be neglected in the present section.

The bare Hamiltonian comprises two terms; the first one (\mathcal{H}_0) includes the contributions which are diagonal in the $l\mathbf{k}$ representation, and the second one (H'_0) the off-diagonal contributions coming from the single-particle potential $\Delta(\mathbf{k}) = e^{i\phi_0}|\Delta(\mathbf{k})|$:

$$H_0 = \sum_{l'l'\mathbf{k}\sigma} H_0^{ll'}(\mathbf{k}) l_{\mathbf{k}\sigma}^\dagger l'_{\mathbf{k}\sigma}, \quad (2)$$

$H_0^{cc}(\mathbf{k}) \equiv \varepsilon_c(\mathbf{k})$, $H_0^{\underline{c}\underline{c}}(\mathbf{k}) \equiv \varepsilon_{\underline{c}}(\mathbf{k})$ and $H_0^{c\underline{c}}(\mathbf{k}) = \Delta(\mathbf{k})$. The transformations

$$l_{\mathbf{k}\sigma}^\dagger = \sum_L U_{\mathbf{k}}(l, L) L_{\mathbf{k}\sigma}^\dagger, \quad (3)$$

lead to

$$H_0 = \sum_{L\mathbf{k}\sigma} E_L(\mathbf{k}) L_{\mathbf{k}\sigma}^\dagger L_{\mathbf{k}\sigma}, \quad (4)$$

with the dispersions

$$E_{\underline{C},C}(\mathbf{k}) = \frac{1}{2}[\varepsilon_{\underline{c}}(\mathbf{k}) + \varepsilon_c(\mathbf{k})] \pm \sqrt{\frac{1}{4}\varepsilon_{\underline{c}c}^2(\mathbf{k}) + |\Delta(\mathbf{k})|^2}. \quad (5)$$

The transformation-matrix elements are given by

$$\begin{pmatrix} U_{\mathbf{k}}(c, C) & U_{\mathbf{k}}(c, \underline{C}) \\ U_{\mathbf{k}}(\underline{c}, C) & U_{\mathbf{k}}(\underline{c}, \underline{C}) \end{pmatrix} = \begin{pmatrix} \cos \frac{\varphi(\mathbf{k})}{2} & e^{-i\phi_0} \sin \frac{\varphi(\mathbf{k})}{2} \\ -e^{i\phi_0} \sin \frac{\varphi(\mathbf{k})}{2} & \cos \frac{\varphi(\mathbf{k})}{2} \end{pmatrix}, \quad (6)$$

where

$$\tan \varphi(\mathbf{k}) = \frac{2|\Delta(\mathbf{k})|}{\varepsilon_{\underline{c}c}(\mathbf{k})}, \quad (7)$$

and $\varepsilon_{\underline{c}c}(\mathbf{k}) = \varepsilon_{\underline{c}}(\mathbf{k}) - \varepsilon_c(\mathbf{k})$.

In the $L\mathbf{k}$ representation, one can write

$$H'_1 = \sum_{LL'\mathbf{k}\mathbf{k}'\sigma} V^{LL'}(\mathbf{k}, \mathbf{k}') L_{\mathbf{k}\sigma}^\dagger L'_{\mathbf{k}'\sigma}, \quad (8)$$

$$H^{\text{ext}} = \sum_{LL'\mathbf{k}\sigma} \left\{ \left[-\frac{1}{c} A_\alpha(\mathbf{q}) J_\alpha^{LL'}(\mathbf{k}) + \delta_{L,L'} \frac{e^2}{2mc} \times A_\alpha^2(\mathbf{q}) \gamma_{\alpha\alpha}^{LL}(\mathbf{k}; 2) \right] L_{\mathbf{k}+\mathbf{q}\sigma}^\dagger L'_{\mathbf{k}\sigma} + \text{h.c.} \right\}. \quad (9)$$

The electromagnetic fields are described in terms of the transverse vector potential $A_\alpha(\mathbf{r})$ polarized in the α direction ($A_\alpha(\mathbf{q})$ and $A_\alpha^2(\mathbf{q})$ are the Fourier transforms of $A_\alpha(\mathbf{r})$ and $A_\alpha^2(\mathbf{r})$, respectively), while $J_\alpha^{LL'}(\mathbf{k})$ and $\gamma_{\alpha\alpha}^{LL}(\mathbf{k}; 2)$ are the related current and bare Raman vertex functions (see Appendix A).

The memory-function approach will be applied now to the Hamiltonian (1).

2. Current-current correlation functions

The retarded current-current correlation functions are defined by [25]

$$\Pi_{\alpha\alpha}^{LL'}(\mathbf{q}, z) = \frac{1}{\hbar V} \langle \langle \hat{J}_\alpha^{LL'}(\mathbf{q}); \hat{J}_\alpha^{L'L}(-\mathbf{q}) \rangle \rangle_z, \quad (10)$$

with $\hat{J}_\alpha^{LL'}(\mathbf{q})$ representing the current density operator

$$\begin{aligned} \hat{J}_\alpha^{LL'}(\mathbf{q}) &= \sum_{\mathbf{k}\sigma} \hat{J}_\alpha^{LL'}(\mathbf{k}, \mathbf{k}_+), \\ \hat{J}_\alpha^{LL'}(\mathbf{k}, \mathbf{k}_+) &= J_\alpha^{LL'}(\mathbf{k}) L_{\mathbf{k}\sigma}^\dagger L'_{\mathbf{k}+\mathbf{q}\sigma}. \end{aligned} \quad (11)$$

Here \mathbf{k}_+ is the abbreviation for $\mathbf{k} + \mathbf{q}$, $z = \hbar\omega + i\eta$ and $\langle \langle \hat{A}; \hat{B} \rangle \rangle_z$ labels the retarded correlation function of the density operators \hat{A} and \hat{B} :

$$\begin{aligned} \langle \langle \hat{A}; \hat{B} \rangle \rangle_z &= \int_{-\infty}^{\infty} dt e^{-izt/\hbar} \langle \langle \hat{A}; \hat{B} \rangle \rangle_t, \\ \langle \langle \hat{A}; \hat{B} \rangle \rangle_t &= -i\Theta(t) \langle [\hat{A}(t), \hat{B}] \rangle \end{aligned} \quad (12)$$

($\hat{A}(t)$ is the Heisenberg representation of \hat{A}).

In order to determine $\Pi_{\alpha\alpha}^{LL'}(\mathbf{q}, z)$, which is now a rather complicated function of various scattering terms (H'_0 , H'_1 or H'_2), one usually starts with the equation of motion for the correlation function

$$\mathcal{D}_1^{LL'}(\mathbf{k}, \mathbf{k}', \mathbf{q}, t) = \langle \langle \hat{J}_\alpha^{LL'}(\mathbf{k}, \mathbf{k}_+); \hat{J}_\alpha^{L'L}(\mathbf{k}', \mathbf{k}'_+) \rangle \rangle_t, \quad (13)$$

which gives

$$\begin{aligned} z_{LL'}(\mathbf{k}) \mathcal{D}_1^{LL'}(\mathbf{k}, \mathbf{k}', \mathbf{q}, z) &= \delta_{\mathbf{k}, \mathbf{k}'} \hbar |J_\alpha^{LL'}(\mathbf{k})|^2 [f_L(\mathbf{k}) - f_{L'}(\mathbf{k}_+)] - \frac{1}{z_{LL'}(\mathbf{k}')} \\ &\times [\mathcal{D}_2^{LL'}(\mathbf{k}, \mathbf{k}', \mathbf{q}, z_{LL'}(\mathbf{k}')) - \mathcal{D}_2^{LL'}(\mathbf{k}, \mathbf{k}', \mathbf{q}, 0)]. \end{aligned} \quad (14)$$

The first term on the right-hand side of this expression is relevant only for the interband processes, and consequently was absent in the previous memory-function analyses [15, 25, 26, 27]. In this term the effects of H'_0 on the photon absorption/emission are described using the exact diagonalization of the single-particle problem, Eqs. (2)–(7), with the momentum conservation in the interband current vertices fulfilled due to \mathbf{Q} in H'_0 . On the

other hand, the second term defines the intraband relaxation function, treating the relaxation processes (proportional to $(H')^2$, $H' \approx H'_1$) in the way similar to the Boltzmann equations [31, 32].

Here $\mathcal{D}_2^{LL'}(\mathbf{k}, \mathbf{k}', \mathbf{q}, z_{LL'}(\mathbf{k}'))$ is the force-force correlation function [25, 27, 33] associated with the current-current correlation function $\mathcal{D}_1^{LL'}(\mathbf{k}, \mathbf{k}', \mathbf{q}, z)$:

$$\begin{aligned} \mathcal{D}_2^{LL'}(\mathbf{k}, \mathbf{k}', \mathbf{q}, z_{LL'}(\mathbf{k}')) &= \langle \langle [\hat{J}_\alpha^{LL'}(\mathbf{k}, \mathbf{k}_+), H']; [\hat{J}_\alpha^{L'L}(\mathbf{k}', \mathbf{k}'_+), H'] \rangle \rangle_{z_{LL'}(\mathbf{k}')} \end{aligned} \quad (15)$$

Furthermore, $z_{LL'}(\mathbf{k}) = z + E_L(\mathbf{k}) - E_{L'}(\mathbf{k}_+)$ and $f_L(\mathbf{k}) = [1 + e^{\beta[E_L(\mathbf{k}) - \mu]}]^{-1}$ is the Fermi-Dirac distribution function.

3. High-frequency limit

It is rather a good approximation to retain in the interband relaxation function only self-energy contributions [21], show this term in the form $-i\eta_{\text{inter}} \mathcal{D}_1^{LL'}(\mathbf{k}, \mathbf{k}', \mathbf{q}, z)$, neglect in Eq. (14) the terms which are proportional to \mathbf{q} and, finally, focus attention on the simplest form of the scattering Hamiltonian where the interactions $V^{CC}(\mathbf{k}, \mathbf{k}')$ are time-independent.

The leading contributions in H' to $\mathcal{D}_1^{LL'}(\mathbf{k}, \mathbf{k}', \mathbf{q}, z)$ are given now by

$$\begin{aligned} z \mathcal{D}_1^{CC}(\mathbf{k}, \mathbf{k}', \mathbf{q}, z) &= -\frac{1}{z} [\mathcal{D}_2^{CC}(\mathbf{k}, \mathbf{k}', \mathbf{q}, z) - \mathcal{D}_2^{CC}(\mathbf{k}, \mathbf{k}', \mathbf{q}, 0)], \\ \mathcal{D}_1^{CC}(\mathbf{k}, \mathbf{k}', \mathbf{q}, z) &= \delta_{\mathbf{k}, \mathbf{k}'} |J_\alpha^{CC}(\mathbf{k})|^2 \mathcal{D}_{CC}(\mathbf{k}, \mathbf{k}, z), \end{aligned} \quad (16)$$

with the high-frequency intra- and interband current-current correlation functions ($LL' = CC$ and $LL' = CC, \underline{CC}$, respectively) of the form

$$\begin{aligned} z \Pi_{\alpha\alpha}^{\text{intra}, \infty}(z) &= \frac{1}{V} \sum_{\mathbf{k}\mathbf{k}'\sigma} \frac{\langle |V^{CC}(\mathbf{k}, \mathbf{k}')|^2 \rangle}{z} [J_\alpha^{CC}(\mathbf{k}) - J_\alpha^{CC}(\mathbf{k}')]^2 \frac{1}{\hbar} [\mathcal{D}_{CC}(\mathbf{k}, \mathbf{k}', z) - \mathcal{D}_{CC}(\mathbf{k}, \mathbf{k}', 0)], \quad (17) \\ \Pi_{\alpha\alpha}^{\text{inter}, \infty}(z) &= \frac{1}{V} \sum_{\mathbf{k}\sigma} [J_\alpha^{CC}(\mathbf{k})]^2 \frac{1}{\hbar} [\mathcal{D}_{C\underline{C}}(\mathbf{k}, \mathbf{k}, z) + \mathcal{D}_{\underline{C}C}(\mathbf{k}, \mathbf{k}, z)] \end{aligned} \quad (18)$$

(the label ∞ stands for the high-frequency limit $\hbar\omega/\eta_{\text{intra}} \gg 1$; η_{intra} is the intraband damping energy to be defined below). All physically relevant contributions are shown here in terms of

$$\begin{aligned} \mathcal{D}_{LL'}(\mathbf{k}, \mathbf{k}', z) &= \langle \langle L_{\mathbf{k}\sigma}^\dagger L'_{\mathbf{k}'\sigma}; L_{\mathbf{k}'\sigma}^\dagger L_{\mathbf{k}\sigma} \rangle \rangle_z \\ &= \hbar \frac{f_L(\mathbf{k}) - f_{L'}(\mathbf{k}')}{z + E_L(\mathbf{k}) - E_{L'}(\mathbf{k}')}. \end{aligned} \quad (19)$$

For example, in the single-impurity-scattering approximation, one obtains $\langle |V^{CC}(\mathbf{k}, \mathbf{k}')|^2 \rangle \approx N_i/N |V^0(\mathbf{k}, \mathbf{k}')|^2$;

N_i is the presumably small number of impurities and $V^0(\mathbf{k}, \mathbf{k}')$ is the scattering potential due to one impurity [33]. The generalization of Eq. (17) to the case where the interactions $V^{CC}(\mathbf{k}, \mathbf{k}')$ are time-dependent or where the two-particle scattering term H'_2 is taken into account explicitly is straightforward and will not be considered here (see, for example, Ref. [25]).

4. Low-frequency limit

In the memory-function approach to the normal metallic state, the low-frequency current-current correlation functions come on collecting the most singular scattering events in powers of $(H')^2/\omega$. The standard procedure [25] is based on the intraband memory (or relaxation) function which is defined by

$$M_\alpha(z) = -\frac{mz\Pi_{\alpha\alpha}^{\text{intra},\infty}(z)}{e^2 n_{\text{intra},\alpha}^{\text{eff}}}. \quad (20)$$

$n_{\text{intra},\alpha}^{\text{eff}}$ is the effective number of conduction electrons [34, 35]

$$\begin{aligned} n_{\text{intra},\alpha}^{\text{eff}} &= \frac{m}{e^2} \frac{1}{V} \sum_{\mathbf{k}\sigma} [J_\alpha^{CC}(\mathbf{k})]^2 (-) \frac{\partial f_C(\mathbf{k})}{\partial E_C(\mathbf{k})} \\ &\equiv \frac{1}{V} \sum_{\mathbf{k}\sigma} \gamma_{\alpha\alpha}^{CC}(\mathbf{k}) f_C(\mathbf{k}), \end{aligned} \quad (21)$$

with $\gamma_{\alpha\alpha}^{CC}(\mathbf{k})$ being the static Raman vertex, Eq. (A6).

In the metallic systems with the anisotropic electron dispersion, the numerator of Eq. (20) has a complicated structure. Nevertheless, for $\hbar\omega \rightarrow 0$, a formal decoupling of two integrals in the expression (17) is possible if the average-inverse-relaxation-time approximation is applied. In this case, the inverse relaxation time

$$\begin{aligned} \frac{\hbar}{\tau_{\text{intra}}(\mathbf{k})} &\approx \sum_{\mathbf{k}'} \langle |V^{CC}(\mathbf{k}, \mathbf{k}')|^2 \rangle [1 - J_\alpha^{CC}(\mathbf{k}')/J_\alpha^{CC}(\mathbf{k})] \\ &\quad \times 2\pi\delta[E_C(\mathbf{k}') - \mu] \end{aligned} \quad (22)$$

is averaged over the Fermi surface, resulting in the intraband damping energy

$$\eta_{\text{intra}} = \text{Im}\{M_\alpha(0 + i\eta)\} = \left\langle \frac{\hbar}{\tau_{\text{intra}}(\mathbf{k})} \right\rangle. \quad (23)$$

Finally, the resulting intra- and interband current-current correlation functions read as

$$\begin{aligned} \Pi_{\alpha\alpha}^{\text{intra}}(\hbar\omega) &\approx -\frac{e^2 n_{\text{intra},\alpha}^{\text{eff}}}{m} \frac{i\eta_{\text{intra}}}{\hbar\omega + i\eta_{\text{intra}}}, \\ \Pi_{\alpha\alpha}^{\text{inter}}(\hbar\omega) &\approx \Pi_{\alpha\alpha}^{\text{inter},\infty}(\hbar\omega + i\eta_{\text{inter}}). \end{aligned} \quad (24)$$

A more rigorous treatment of the intraband relaxation processes should include the explicit numerical calculation of two coupled integrals in the expression (17); however, this is beyond the scope of the present work.

C. Optical conductivity

Due to causality, the structure of the multi-component optical conductivity comes on combining the expressions for the current-current correlation functions obtained for $\eta_i \rightarrow 0$ with the corresponding diamagnetic contributions, and replacing η_i with the frequency-independent damping energies $\hbar\Gamma_i$ (representing the single-impurity relaxations for the usual impurity concentrations as well as the other relaxation processes not considered in the $\eta_i \rightarrow 0$ model) [19, 33]. Depending on the ratio among the band parameters, this procedure will result in different optical-conductivity expressions. The two-component optical conductivity (where $2\Delta^0/E_g \approx 1$) and the generalized Drude formula ($2\Delta^0/E_g \ll 1$) are the most interesting cases.

As a first approximation it seems natural to interpret the optical conductivity of (TMTSF)₂PF₆ in terms of the two-component model with the correlation energy scale $2\Delta^0$ comparable to the threshold energy E_g , and with both $\hbar\Gamma_{\text{intra}}$ and $\hbar\Gamma_{\text{inter}}$ independent of frequency. The total optical conductivity $\sigma_\alpha^{\text{total}}(\omega)$ is the sum of the intra- and interband contributions, which are given by the gauge-invariant expressions [11, 19, 36]

$$\sigma_\alpha^{\text{intra}}(\omega) = \frac{i}{\omega} \frac{e^2 n_{\text{intra},\alpha}^{\text{eff}}}{m} \frac{\hbar\omega}{\hbar\omega + i\hbar\Gamma_{\text{intra}}}, \quad (25)$$

$$\begin{aligned} \sigma_\alpha^{\text{inter}}(\omega) &= \frac{i}{\omega} \frac{1}{V} \sum_{\mathbf{k}\sigma} \frac{(\hbar\omega)^2 |J_\alpha^{CC}(\mathbf{k})|^2}{E_{\underline{C}\underline{C}}^2(\mathbf{k})} \\ &\quad \times \left\{ \frac{f_C(\mathbf{k}) - f_{\underline{C}}(\mathbf{k})}{\hbar\omega - E_{\underline{C}\underline{C}}(\mathbf{k}) + i\hbar\Gamma_{\text{inter}}} \right. \\ &\quad \left. + \frac{f_{\underline{C}}(\mathbf{k}) - f_C(\mathbf{k})}{\hbar\omega + E_{\underline{C}\underline{C}}(\mathbf{k}) + i\hbar\Gamma_{\text{inter}}} \right\}, \end{aligned} \quad (26)$$

$$E_{\underline{C}\underline{C}}(\mathbf{k}) = E_{\underline{C}}(\mathbf{k}) - E_C(\mathbf{k}).$$

Since the residual scattering processes (corresponding primarily to the frequency-dependent contributions in H'_1 , or to the two-particle term H'_2) become increasingly pronounced at low frequencies, the intraband contribution (25) should in principle be replaced by the generalized Drude formula

$$\sigma_\alpha^{\text{intra}}(\omega) = \frac{i\hbar e^2 n_{\text{intra},\alpha}^{\text{eff}}/m}{\hbar\omega(m(\omega)/m) + i\text{Im}\{M_\alpha(\hbar\omega + i\eta)\}}. \quad (27)$$

The total optical conductivity is now the sum of the expressions (27) and (26). Here $m(\omega)$ results from the Kramers-Kronig relations, with $H' = H'_1 + H'_2$ in Eq. (20). Similarly, in the limit $2\Delta^0/E_g \ll 1$, one obtains the generalized Drude expression $\sigma_\alpha^{\text{total}}(\omega) \approx \sigma_\alpha^{\text{intra}}(\omega)$ with $H' = H'_0 + H'_1 + H'_2$ and $\sigma_\alpha^{\text{intra}}(\omega)$ given by Eq. (27).

It should be noted that the direct integration of the real part of the expressions (25) and (26) gives rise to the intraband, interband and total spectral weights of the form [19, 37]

$$\frac{1}{2} \Omega_{i,\alpha}^2 = \frac{m_{\text{aa}}}{m} V_0 n_{i,\alpha}^{\text{eff}} \frac{m}{m_{\text{aa}}} \frac{1}{2} \Omega_0^2, \quad (28)$$

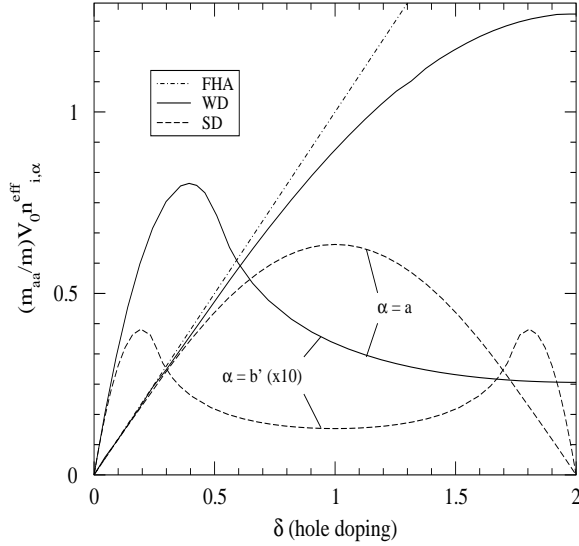


FIG. 2: The development of the effective number of conduction electrons with doping for the $\Delta^0 = 0$ WD and SD models. The dot-dashed line is the prediction of the free-hole approximation (FHA). $t_a = 0.25$ eV, $t_{b'} = 25$ meV (WD case) and $\tilde{t}_a = 0.125$ eV, $t_{b'} = 12.5$ meV (SD case). For clarity, the $\alpha = b'$ effective numbers are multiplied by a factor of 10.

where $i \in \{\text{intra, inter, total}\}$. The effective total number of electrons is given by

$$n_{\text{total},\alpha}^{\text{eff}} = \frac{1}{V} \sum_{\mathbf{k}\sigma} \gamma_{\alpha\alpha}^{CC}(\mathbf{k}; 2) f_C(\mathbf{k}), \quad (29)$$

$n_{\text{inter},\alpha}^{\text{eff}} = n_{\text{total},\alpha}^{\text{eff}} - n_{\text{intra},\alpha}^{\text{eff}}$ and $n_{\text{intra},\alpha}^{\text{eff}}$ comes from Eq. (21). Furthermore, $\Omega_0 = \sqrt{4\pi e^2/(mV_0)}$ is an auxiliary frequency scale which represents the bare plasma frequency attributed to the free holes with the concentration $n = 1/V_0$, $m_{aa} = 2\hbar^2/(t_a a^2)$ is the mass parameter and the $(m_{aa}/m)V_0 n_{i,\alpha}^{\text{eff}}$ are the effective numbers shown in a convenient dimensionless form.

Before turning to the detailed numerical calculation, let us consider the total spectral weights and remember the estimates of the bond-energies in (TMTSF)₂PF₆ [2, 11]. It has been established that the measured plasma energy $\hbar\Omega_{\text{total},a}$ (1.1–1.4 eV [1, 2, 3, 4]) is close to the energy $\hbar\Omega_0 \approx 1.385$ eV (or $\Omega_0/(2\pi c) \approx 1.1 \cdot 10^4$ cm⁻¹). Using the $\Delta^0 = 0$ WD model [2] this observation has led to the conclusion that the bond-energy $t_a \approx t_a^0$, where $t_a^0 \approx 0.285$ eV is the characteristic bond-energy for which the mass parameter m_{aa} is equal to the bare electron/hole mass m . Similarly, for $\delta \approx 1$ (corresponding to the open Fermi surface), one obtains [38]

$$n_{\text{total},b'}^{\text{eff}} \approx \beta \frac{t_{b'}^2}{t_a^2} n_{\text{total},a}^{\text{eff}}, \quad (30)$$

with $\beta \approx 4$ for the $\Delta^0 = 0$ WD case (see Fig. 2). For $t_{b'} = 0.1t_a$, this has resulted in the bare plasma frequency $\Omega_{\text{total},b'} \approx 0.2\Omega_{\text{total},a}$ which agrees reasonably well with measured values [2, 3, 4].

Due to the scattering term H'_0 , for $\mathbf{Q} \approx 2\mathbf{k}_F$ the quantities $n_{\text{intra},\alpha}^{\text{eff}}$ and $\Pi_{\alpha\alpha}^{\text{intra},\infty}(z)$ are strongly reduced with respect to their values in the free-hole approximation. In addition, the analytical decoupling of two integrals in $\Pi_{\alpha\alpha}^{\text{intra},\infty}(z)$ can be achieved only using the average-inverse-relaxation-time approximation ($-\hbar\omega \text{Im}\{\Pi_{\alpha\alpha}^{\text{intra},\infty}(\hbar\omega + i\eta)\} \approx \hbar\Gamma_{\text{intra}} e^2 n_{\text{intra},\alpha}^{\text{eff}}/m$). For this reason, from here on we will focus the attention on the two-component model (25)–(26) only, with the damping energies independent of frequency and with $\Delta(\mathbf{k}) = \Delta^0$.

Leaving the factors m/m_{aa} and $\Omega_0^2/2$ in Eq. (28) off, the total spectral weight is calculated now as a function of the doping level for the bond-energies $t_a = 0.25$ eV, $t_{b'} = 25$ meV (WD case) and $\tilde{t}_a = 0.125$ eV, $t_{b'} = 12.5$ meV (SD case) and for the photon polarizations $\alpha = a$ and $\alpha = b'$, and shown in Fig. 2. Although the SD model, when fitted to the measured total spectral weights, will result in the slightly different values of the bond-energies, on the qualitative side (for not too large $\Delta^0/(2\tilde{t}_a)$ and $\hbar\omega/(2\tilde{t}_a)$) there is no essential difference between these two models in explaining the structure of the $\Delta^0 \neq 0$ optical conductivity. In this respect, we continue the analysis considering the SD model, and assuming that $\hbar\omega, k_B T, \Delta^0, t_{b'}, \hbar\Gamma_i \ll 2\tilde{t}_a$. It is important to notice that the model (25)–(26) for $t_{b'} \rightarrow 0$ is essentially the same as the strictly 1D spinless-fermion optical model of Pedron et al. [11], and, not surprisingly, the present estimates of t_a , Δ^0 and $\hbar\Gamma_i$ will be close to their estimated values. However, there is a pronounced qualitative difference between these two optical models regarding the Fermi energy and wave vector positions ($\mathbf{Q} \approx 2\mathbf{k}_F$ here, contrary to $\mathbf{Q} \approx 4\mathbf{k}_F$ in the spinless-fermion model).

III. COMPARISON WITH EXPERIMENTS

The optical anomalies of (TMTSF)₂PF₆ mentioned in Section 1 will be analyzed now in the framework of the Q1D fermionic model (25)–(26). The competition between the small energy scales of this model, which results in the structures in the optical conductivity similar to that observed in experiments, is the focus of the present discussion. We consider first a few general features which emerge as a result of this competition. Then the model parameters suitable to the $T = 100$ K spectra of (TMTSF)₂PF₆ will be discussed in more detail. In the rest of the text the full notation is used with the index $m = 2$, in Δ_2^0 and E_{g2} , written explicitly.

A. Competition between $t_{b'}$ and Δ_2^0

The $\alpha = a$ conductivity sum rule of the present two-component model, $\Omega_{\text{total},a}^2 = \Omega_{\text{intra},a}^2 + \Omega_{\text{inter},a}^2$, does not depend on the damping energies $\hbar\Gamma_i$. The main consequences of the interplay between $t_{b'}$ and Δ_2^0 can be thus seen from Fig. 3, where the effective numbers $n_{\text{intra},\alpha}^{\text{eff}}$

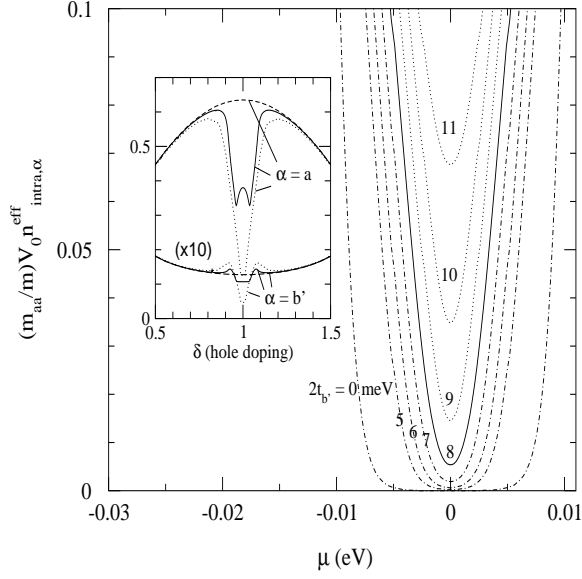


FIG. 3: Main figure: The $\alpha = a$ intraband spectral weight as a function of the chemical potential μ for different values of $2t_{b'}$ ($2t_{b'} = 0$ and $5 - 11$ meV, $2\tilde{t}_a = 0.25$ eV, $\Delta_2^0 = 10$ meV and $T = 10$ K). Inset of figure: The dependence of $n_{\text{intra},\alpha}^{\text{eff}}$ on δ for the $\Delta_2^0 = 0$ (dashed line), $\Delta_2^0 = 10$ meV (solid line) and $\Delta_2^0 = 20$ meV (dotted line) SD models, $2\tilde{t}_a = 0.25$ eV, $2t_{b'} = 25$ meV and $T = 10$ K. The $\alpha = b'$ spectral weight is again multiplied by 10.

are displayed as a function of the crossover parameter $2\Delta_2^0/t_{b'}$ at a relatively small temperature $T = 10$ K. For $t_{b'} \rightarrow 0$ but Δ_2^0 finite, the electrons will be confined on individual chains, as found in the insulating $(\text{TMTTF})_2X$ salts, where $X = \text{PF}_6$ or Br [5]. The effective number $n_{\text{intra},a}^{\text{eff}} \approx n/100$ required to give the metallic behaviour observed in $(\text{TMTSF})_2\text{PF}_6$ is obtained for $2\Delta_2^0/t_{b'} \approx 5$ (main figure, $T = 10$ K). This value is approximately twice the critical value $E_{g2}/t_{b'} = 1.8-2.3$ for the confinement (i.e. for the metal-to-insulator phase transition) obtained by the renormalization group approach for the problem of two coupled chains [18]. The value of $2\Delta_2^0/t_{b'}$ decreases with decreasing temperature, resulting in $2\Delta_2^0/t_{b'} \approx 4$ at $T = 2$ K. Another reason for this discrepancy should be the fact that the ratio $\tilde{t}_a/t_{b'}$ plays important role as well; namely, for \tilde{t}_a fixed, the increase of $t_{b'}$ transforms the Q1D electronic system into an anisotropic 2D system, where the dimerization along the x -axis becomes less important. As illustrated in the inset of the figure, for $2\Delta_2^0/t_{b'}$ small enough, the gap opens only on a part of the Fermi surface resulting for $n_{\text{intra},a}^{\text{eff}}$ in a local maximum at $\delta = 1$. On the contrary, for $2\Delta_2^0/t_{b'} > 2.5$ and $T = 10$ K, the correlation gap develops on the complete Fermi surface, with the bare group velocity $J_a^{cc}(\mathbf{k})/e$ in the effective number of conduction electrons replaced by the “renormalized” one, $J_a^{CC}(\mathbf{k})/e = \cos \varphi(\mathbf{k}) J_a^{cc}(\mathbf{k})/e$, with approximately $\cos \varphi(\mathbf{k}) \approx \cos \varphi(\mathbf{k}_F)$.

The number $n_{\text{intra},b'}^{\text{eff}}$ is affected by the correlations in

the same way as $n_{\text{intra},a}^{\text{eff}}$. While the rest of the $\alpha = a$ total spectral weight, i.e. the difference between the dashed and solid (dotted) line in the inset of Fig. 3, reappears through the coherent excitations across the correlation gap E_{g2} , for $\alpha = b'$ there is no counterpart of these coherent finite-frequency excitations. Therefore, to fulfil the $\alpha = b'$ conductivity sum rule, one has to go beyond the optical model (25)–(26), and to take also incoherent optical processes in the \mathbf{b}' direction into account [39]. Obviously, this issue is of a general importance for the complete quantitative description of the optical conductivity of the Bechgaard salts, and should be in relation with the disappearance of the plasma edge in the $\alpha = b'$ reflectivity spectra of the $(\text{TMTTF})_2X$ salts [5].

B. Relation with the CDW systems and the high- T_c cuprates

Besides the dramatic dependence on the crossover parameter $2\Delta_2^0/t_{b'}$, the optical model (25)–(26) exhibits also various temperature-dependent features, due to the competition between the energies $k_B T$, $\Delta_2^0(T)$ and $\hbar\Gamma_{\text{inter}}(T)$. Some of these temperature effects are at first sight similar to the anomalies (i)–(iv) mentioned in Section 1. Interestingly, they are more directly related to different MIR optical features observed in various other Q1D and 2D systems. To compare briefly the predictions of the model with the MIR spectra measured in the CDW systems in the ordered ground state [7], as well as in the normal metallic state of the underdoped high- T_c cuprates [8, 9, 10], we apply it now to the insulating $\delta = 1$, $t_{b'} \rightarrow 0$ case.

The real part of the intraband conductivity has the usual form $\text{Re}\{\sigma_a^{\text{intra}}(\omega)\} = \sigma_a^{\text{DC}}/(1 + (\omega/\Gamma_{\text{intra}})^2)$. $\sigma_a^{\text{DC}} = \Omega_0^2 V_0 n_{\text{intra},a}^{\text{eff}}/(4\pi\Gamma_{\text{intra}})$ is the DC conductivity, which vanishes at $T = 0$ K. The temperature dependence of σ_a^{DC} is governed by the thermal activation of the conduction electrons, according to the expression

$$n_{\text{intra},a}^{\text{eff}} = \frac{1}{V} \sum_{\mathbf{k}\sigma} \gamma_{aa}^{CC}(\mathbf{k}) [f_C(\mathbf{k}) - f_{\underline{C}}(\mathbf{k})]. \quad (31)$$

This temperature dependence is accompanied by the decrease of the interband spectral weight, as seen from

$$\begin{aligned} \text{Re}\{\sigma_a^{\text{inter}}(\omega)\} &= \frac{1}{\omega} \frac{1}{V} \sum_{\mathbf{k}\sigma} \frac{(\hbar\omega)^2 |J_a^{CC}(\mathbf{k})|^2}{E_{\underline{C}\underline{C}}^2(\mathbf{k})} \\ &\times \frac{4\hbar\omega E_{\underline{C}\underline{C}}(\mathbf{k})}{[\hbar\omega + E_{\underline{C}\underline{C}}(\mathbf{k})]^2 + \hbar\Gamma_{\text{inter}}^2} \\ &\times \frac{\hbar\Gamma_{\text{inter}} [f_C(\mathbf{k}) - f_{\underline{C}}(\mathbf{k})]}{[\hbar\omega - E_{\underline{C}\underline{C}}(\mathbf{k})]^2 + \hbar\Gamma_{\text{inter}}^2}, \quad (32) \end{aligned}$$

where the same temperature factor can be recognized ($f_C(\mathbf{k}) - f_{\underline{C}}(\mathbf{k}) \approx \tanh[E_{\underline{C}}(\mathbf{k})/(2k_B T)]$ for $\mu = 0$).

It should be interesting first to remember that the optical model (32) with $\Delta_2^0 \rightarrow \Delta_{\text{CDW}}$ gives a correct

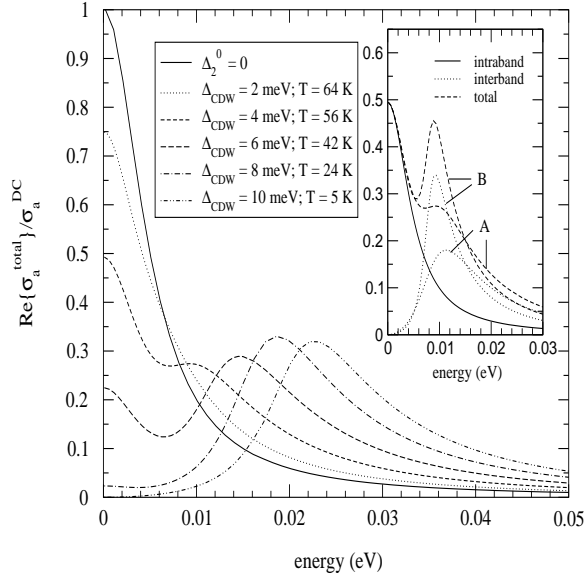


FIG. 4: The dependence of the real part of the $\alpha = a$ optical conductivity on $k_B T$, for $\delta = 1$, $2\tilde{t}_a = 0.25$ eV, $t_{b'} \rightarrow 0$ and $\hbar\Gamma_{\text{intra}} = 5$ meV. Main figure: The temperature dependence of the spectra for $\Delta_2^0 \rightarrow \Delta_{\text{CDW}} \leq 10$ meV and $\hbar\Gamma_{\text{inter}} = 5$ meV (underdamped regime). σ_a^{DC} is the DC conductivity of the metallic $\Delta_2^0 = 0$ state, and the solid line is the related optical conductivity. Inset of figure: The dependence of the total and interband spectra on $\hbar\Gamma_{\text{inter}}$: $\Delta_{\text{CDW}} = 4$ meV, $T = 56$ K, $\hbar\Gamma_{\text{intra}} = 5$ meV (curves A) and $\hbar\Gamma_{\text{inter}} = 2$ meV (curves B).

prediction for the $T \approx 0$ K subgap conductivity characterizing the ordered CDW systems, due to the gauge-invariance factor $(\hbar\omega)^2/E_{\text{CC}}^2(\mathbf{k})$ [19]. It also provides the correct treatment of the conductivity sum rules, even for the relatively large damping energies, due to the factor $4\hbar\omega E_{\text{CC}}(\mathbf{k})/[(\hbar\omega + E_{\text{CC}}(\mathbf{k}))^2 + \hbar\Gamma_{\text{inter}}^2]$, at variance with the ordinary CDW model [12, 13, 14] which fails in both of these cases.

Fig. 4 illustrates the development of $\text{Re}\{\sigma_a^{\text{total}}(\omega)\}$ with temperature in the CDW ground state for the underdamped case $\Delta_0/(\hbar\Gamma_{\text{inter}}) = 2$. The temperature dependence of the order parameter is modeled by a simple expression $\Delta_{\text{CDW}}(T) \approx \Delta_0 \sqrt{1 - T/T^*}$ (T^* is an auxiliary temperature scale given by $k_B T^* = \Delta_0/1.75$, with $T^* \approx T_{\text{CDW}}$). Interestingly, almost the same temperature behaviour is found for the $\alpha = b'$ optical conductivity in $(\text{TMTSF})_2\text{PF}_6$ at $T < T^* \approx 15$ K, with the SDW (pseudo)gap parameter $2\Delta_0/(\hbar c) \approx 70$ cm^{-1} [6].

Equally important is the observation in the normal metallic state of $\text{Bi}_2\text{Sr}_2\text{CuO}_6$ that the MIR maximum shifts with increasing temperature from $\omega_{\text{peak}}/(2\pi c) \approx 100$ cm^{-1} at $T = 30$ K to $\omega_{\text{peak}}/(2\pi c) \approx 500$ cm^{-1} at $T = 300$ K [9] (with a similar trend found in the $\text{La}_{2-x}\text{Sr}_x\text{CuO}_4$ compounds [10]). This unusual behaviour has been explained using the 1D orbital Kondo model of Emery and Kivelson [16], which predicts $E_{\text{peak}} \approx \hbar\Gamma$. Fig. 5 demonstrates that the same be-

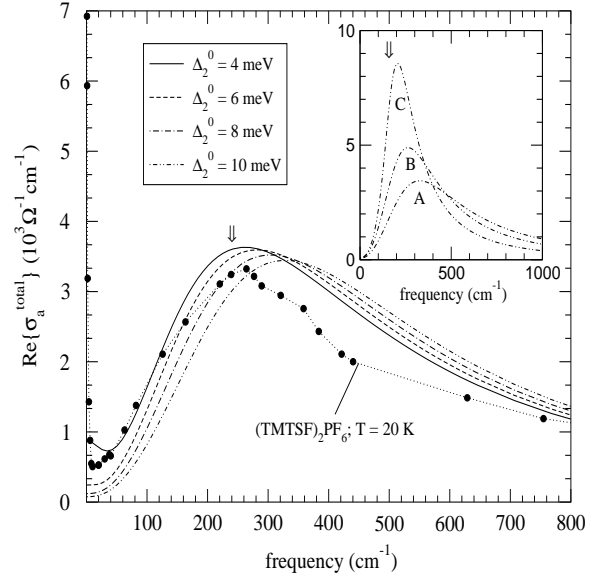


FIG. 5: The dependence of the real part of the $\alpha = a$ optical conductivity on the ratio $\hbar\Gamma_{\text{inter}}/\Delta_2^0$, for $\delta = 1$, $2\tilde{t}_a = 0.25$ eV, $t_{b'} \rightarrow 0$, $\hbar\Gamma_{\text{intra}} = 5$ meV, $T = 10$ K, $m_{aa}/m = 1$ and $\hbar\Omega_2^0/(4\pi \text{ eV}) = 0.355 \cdot 10^3 (\Omega\text{cm})^{-1}$. Main figure: The overdamped regime; $\hbar\Gamma_{\text{inter}} = 30$ meV. The data measured in $(\text{TMTSF})_2\text{PF}_6$ at $T = 20$ K are given for comparison. Inset of figure: The intermediate regime; $\Delta_2^0 = 10$ meV with $\hbar\Gamma_{\text{inter}} = 30, 20$ and 10 meV for the curves A, B and C, respectively. The energies $\hbar\Gamma_{\text{inter}}$ (main figure) and $2\Delta_2^0$ (inset of figure) are indicated by arrows.

haviour emerges in the overdamped regime of the model (25)–(26): $\hbar\Gamma_{\text{inter}} \gg \Delta_2^0$ leads to $E_{\text{peak}} \approx \hbar\Gamma_{\text{inter}}$. It seems that at least in the compounds mentioned above the unusual temperature dependence of E_{peak} at temperatures up to room temperature has the same origin, the competition between the correlation energy scale in question and the presumably large (interband) damping energy.

In conclusion, in the underdamped regime of the present optical model the position of the maximum in the MIR spectra is close to the threshold energy E_{g2} as well as to the correlation energy scale $2\Delta_2^0$. On the other hand, in the intermediate and overdamped regime one expects to be $E_{\text{peak}}(\Delta_2^0, \hbar\Gamma_{\text{inter}})$, so that the correlation energy $2\Delta_2^0$ cannot be extracted directly from the measured E_{peak} .

C. $(\text{TMTSF})_2\text{PF}_6$

Once the bond-energies t_a and $t_{b'}$, together with the correlation energy scale $2\Delta_2^0$, are estimated from the spectral weights, the damping energies $\hbar\Gamma_{\text{intra}}$ and $\hbar\Gamma_{\text{inter}}$ and the background dielectric function $\varepsilon_{\infty, a}$ are the only free parameters to be estimated from the real part of the optical conductivity and the real part of the dielectric function obtained in experiments.

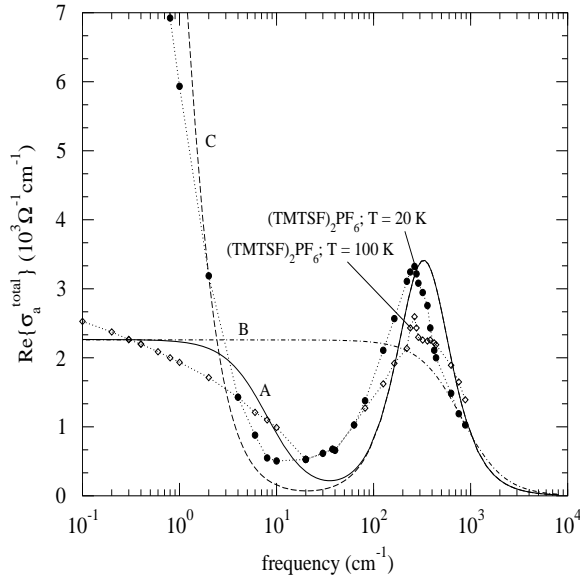


FIG. 6: The real part of the $\alpha = a$ optical conductivity as a function of the intraband damping energy, for the SD model with $n_{\text{intra},a}^{\text{eff}} = n/100$; $2\tilde{t}_a = 0.25$ eV, $2t_{b'} = 8$ meV, $\Delta_2^0 = 10$ meV, $\hbar\Gamma_{\text{inter}} = 30$ meV, $T = 10$ K, $m_{aa}/m = 1$ and $\hbar\Omega_0^2/(4\pi \text{ eV}) = 0.355 \cdot 10^3 (\Omega\text{cm})^{-1}$. $\hbar\Gamma_{\text{intra}} = 1$ and 0.1 meV for the curves A and C, respectively. The prediction of the simple Drude model (curve B, $\Delta_2^0 = 0$ and $\hbar\Gamma_{\text{intra}} = 0.1$ eV) and the typical measured spectra [3] are also shown.

According to the general relation

$$\varepsilon_a(\omega) \approx \varepsilon_{\infty,a}(\omega) + \frac{4\pi i}{\omega} \sigma_a^{\text{total}}(\omega), \quad (33)$$

$\varepsilon_{\infty,a}(\omega) - 1$ describes the contribution of the optical processes not included in the Hamiltonian (1). In the Bechgaard salts, for $\hbar\omega < 1$ eV, it is established that $\text{Im}\{\varepsilon_{\infty,a}(\omega)\} \approx 0$ and $\text{Re}\{\varepsilon_{\infty,a}(\omega)\} = \varepsilon_{\infty,a} \approx 2.5$ [1, 2].

In order to obtain a satisfactory explanation of the estimated damping energies $\hbar\Gamma_i$, it is useful first to remember [25, 40, 41] that the equation of motion (14) generates automatically the self-energy and vertex contributions to the memory functions (i.e. to $\hbar\Gamma_i$). Furthermore, it should be noticed that omitting the vertex corrections makes the damping energies $\hbar\Gamma_{\text{intra}}$ and $\hbar\Gamma_{\text{inter}}$ appear as two limiting cases of a frequency-dependent relaxation function $\hbar\Gamma(\hbar\omega)$ which describes the pseudogap effects in the electron self-energy ($\hbar\Gamma_{\text{intra}} \approx \hbar\Gamma(0)$ and $\hbar\Gamma_{\text{inter}} \approx \hbar\Gamma(\hbar\omega \gg 2\Delta_2^0)$). Not surprisingly, the function $\hbar\Gamma(\hbar\omega)$ related to the umklapp scattering processes beyond the mean-field approximation adopted here should have the temperature and frequency dependence similar to that found recently for the half-filled spinless Holstein model in which the CDW (pseudo)gap features have been studied [20].

The dependence of $\text{Re}\{\sigma_a^{\text{total}}(\omega)\}$ and $\text{Re}\{\varepsilon_a^{\text{total}}(\omega)\}$ on the damping energies $\hbar\Gamma_i$ for the SD case with $n_{\text{intra},a}^{\text{eff}} = n/100$ is shown in Figs. 6 and 7, and compared to the experimental data. According to the questions raised in

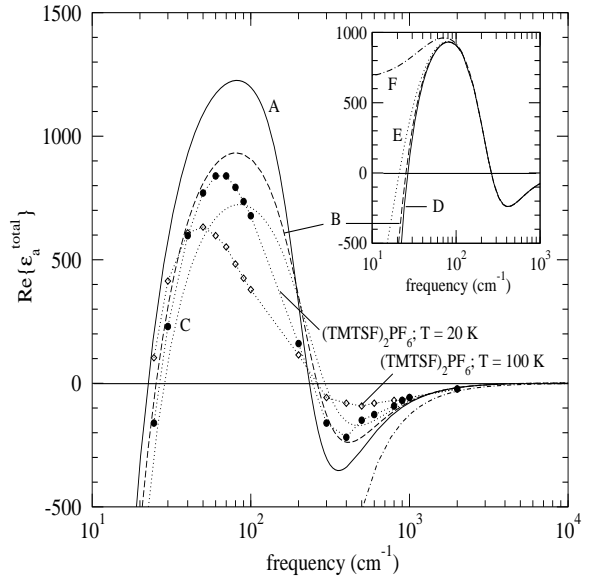


FIG. 7: The dependence of the real part of the $\alpha = a$ dielectric function on $\hbar\Gamma_{\text{inter}}$ (main figure) and $\hbar\Gamma_{\text{intra}}$ (inset of figure), for $2\tilde{t}_a = 0.25$ eV, $2t_{b'} = 8$ meV, $\Delta_2^0 = 10$ meV, $T = 10$ K, $m_{aa}/m = 1$, $\hbar\Omega_0 = 1.4$ eV and $\varepsilon_{\infty,a} = 2.5$. Main figure: $\hbar\Gamma_{\text{intra}} = 1$ meV, and $\hbar\Gamma_{\text{inter}} = 15, 20$ and 25 meV for the curves A, B and C, respectively. The dot-dashed line describes the $\Delta_2^0 = 0$ case. Inset of figure: $\hbar\Gamma_{\text{inter}} = 20$ meV and $\hbar\Gamma_{\text{intra}} = 0.1, 1, 2$ and 5 meV (D, B, E and F). The experimental data are from Ref. [3].

Section 1, the most important qualitative conclusions are as follows.

The power-law frequency dependence $\text{Re}\{\sigma_a^{\text{total}}(\omega)\} \propto \omega^{-\nu}$, $\nu \approx 1.3$, for frequencies greater than E_{peak}/\hbar , observed at $T < 20$ K, is well understood as a direct consequence of the umklapp scattering processes [4, 5, 15]. On the other hand, the temperature dependence of both ν and E_{peak} , in particular at temperatures above 100 K, indicates the regime where $\hbar\Gamma_{\text{inter}}$ is comparable with $2\Delta_2^0$, and, consequently, where the temperature effects are primarily due to $\hbar\Gamma_{\text{inter}}(T)$, as shown in the inset of Fig. 5. Therefore, the energy $\hbar\Gamma_{\text{inter}} \approx 25\text{--}30$ meV represents roughly the high-frequency limit of the relaxation function $\hbar\Gamma(\hbar\omega)$. On the other hand, the zero-frequency limit reveals the energy $\hbar\Gamma_{\text{intra}} \approx 1$ meV at $T = 100$ K, indicating the strong pseudogap effects, with an additional, pronounced decrease on decreasing temperature ($\hbar\Gamma_{\text{intra}} \approx 0.1$ meV at $T = 20$ K). To improve the overall agreement between the model predictions and the measured spectra, including the anomalous frequency dependence of the Drude peak as well as the temperature dependence of its spectral weight, it is necessary to take into account the frequency dependence of the damping energies in Eqs. (25)–(26). When considering the two-component model with the causality properties treated correctly, this problem, however, requires a more accurate and extensive investigation and will not be discussed here.

According to Fig. 7, there are two zeros of $\text{Re}\{\varepsilon_a(\omega)\}$, representing the motion of two different plasma modes. These frequencies are related to the frequencies $\Omega_{i,a}$ estimated from the spectral weights. Not surprisingly, a simple Drude relation $\omega_{\text{pl},a}^i \approx \Omega_{i,a}/\sqrt{\varepsilon_{\infty,a}}$ is not valid here. In this respect, the total plasma frequency $\omega_{\text{pl},a}^{\text{total}}/(2\pi c) \approx 0.55 \cdot 10^4 \text{ cm}^{-1}$ has to be compared to the plasma frequency $\Omega_0/(2\pi c\sqrt{\varepsilon_{\infty,a}}) \approx 0.7 \cdot 10^4 \text{ cm}^{-1}$ of the $\Delta_2^0 = 0$ case, and to the bare plasma frequency $\Omega_0/(2\pi c) \approx 1.1 \cdot 10^4 \text{ cm}^{-1}$ corresponding to $\Delta_2^0 = 0$, $\varepsilon_{\infty,a} = 1$. Similarly, $\omega_{\text{pl},a}^{\text{intra}}/(2\pi c) \approx 20 \text{ cm}^{-1}$, in contrast to $\Omega_{\text{intra},a}/(2\pi c) \approx 10^3 \text{ cm}^{-1}$. Furthermore, a pronounced dependence of $\omega_{\text{pl},a}^{\text{intra}}$ on $\hbar\Gamma_{\text{intra}}$ for $\Gamma_{\text{intra}} > \omega_{\text{pl},a}^{\text{intra}}$ can also be noticed in the inset of figure.

IV. CONCLUSION

To summarize, we have formulated a gauge invariant approach to the optical conductivity of the Q1D interacting electronic systems with a MIR structure clearly distinguished from both the zero-frequency (Drude-like) and the high-frequency (background) contributions. By using the simplest limit of this model, with the frequency-independent damping energies, the confinement of the conduction electrons to the highly conducting chains is analyzed. The estimated ratio $2\Delta_2^0/t_b$ required to give the spectral weights measured in $(\text{TMTSF})_2\text{PF}_6$ agrees with the conclusions of the previous renormalization-group study.

The real part of the optical conductivity is calculated for the typical insulating and metallic state, giving rise to a satisfactory agreement with the experimental findings at temperatures well above T_{SDW} . The estimated damping energies clearly show the (pseudo)gap features in the charge excitation spectrum and are in a qualitative agreement with the relaxation function calculated recently for the systems with the CDW ground state. However, to obtain a better fit to the measured data, even at $T \gg T_{\text{SDW}}$, one has to go beyond the present model and to treat the umklapp scattering processes dynamically.

Two plasma modes are found in the metallic state, with a nontrivial relation between their frequencies and the corresponding spectral weights.

Acknowledgement

This research was supported by the Croatian Ministry of Science and Technology under the project 0119-256.

APPENDIX A: VERTEX FUNCTIONS

To account for the effects of the dimerization/correlation potential on the coupling between the tight-binding electronic system and the electromagnetic fields, we choose the $l\mathbf{k}$ representation, apply the

usual substitution for the electron momentum, and, finally, transform the obtained coupling Hamiltonian in the $L\mathbf{k}$ representation.

Inserting

$$\delta H_0^{ll'}(\mathbf{k}) \approx -\frac{\partial H_0^{ll'}(\mathbf{k})}{\partial k_\alpha} \frac{e}{\hbar c} A_\alpha(\mathbf{q}) + \frac{1}{2} \frac{\partial^2 H_0^{ll'}(\mathbf{k})}{\partial k_\alpha^2} \left(\frac{e}{\hbar c}\right)^2 A_\alpha^2(\mathbf{q}) \quad (\text{A1})$$

in

$$H^{\text{ext}} = \sum_{ll'\mathbf{k}\sigma} \delta H_0^{ll'}(\mathbf{k}) [l_{\mathbf{k}+\mathbf{q}\sigma}^{l'} l_{\mathbf{k}\sigma}' + \text{h.c.}], \quad (\text{A2})$$

we obtain the coupling Hamiltonian given by Eq. (9) in the main text. The intraband bare Raman vertices are of the form

$$\gamma_{\alpha\alpha}^{\underline{CC},CC}(\mathbf{k}; 2) = \frac{m}{2\hbar^2} \left[\frac{\partial^2 [\varepsilon_{\underline{c}}(\mathbf{k}) + \varepsilon_c(\mathbf{k})]}{\partial k_\alpha^2} \pm \cos \varphi(\mathbf{k}) \frac{\partial^2 \varepsilon_{\underline{c}}(\mathbf{k})}{\partial k_\alpha^2} \pm \sin \varphi(\mathbf{k}) \frac{2\partial^2 |\Delta(\mathbf{k})|}{\partial k_\alpha^2} \right] \quad (\text{A3})$$

with the upper (lower) sign in \pm corresponding to \underline{CC} (CC). Similarly, the intra- and interband current vertices are

$$J_{\alpha}^{\underline{CC},CC}(\mathbf{k}) = \frac{e}{2\hbar} \left[\frac{\partial [\varepsilon_{\underline{c}}(\mathbf{k}) + \varepsilon_c(\mathbf{k})]}{\partial k_\alpha} \pm \cos \varphi(\mathbf{k}) \frac{\partial \varepsilon_{\underline{c}}(\mathbf{k})}{\partial k_\alpha} \pm \sin \varphi(\mathbf{k}) \frac{2\partial |\Delta(\mathbf{k})|}{\partial k_\alpha} \right], \quad (\text{A4})$$

$$J_{\alpha}^{\underline{CC}}(\mathbf{k}) = [J_{\alpha}^{\underline{CC}}(\mathbf{k})]^* = -\frac{e}{2\hbar} e^{-i\phi_0} \times \left[\sin \varphi(\mathbf{k}) \frac{\partial \varepsilon_{\underline{c}}(\mathbf{k})}{\partial k_\alpha} - \cos \varphi(\mathbf{k}) \frac{2\partial |\Delta(\mathbf{k})|}{\partial k_\alpha} \right]. \quad (\text{A5})$$

The corresponding static Raman vertices $\gamma_{\alpha\alpha}^{\underline{CC},CC}(\mathbf{k})$ come from the effective mass theorem

$$\begin{aligned} \gamma_{\alpha\alpha}^{\underline{CC},CC}(\mathbf{k}) &= \gamma_{\alpha\alpha}^{\underline{CC},CC}(\mathbf{k}; 2) \pm \frac{2m|J_{\alpha}^{\underline{CC}}(\mathbf{k})|^2}{e^2 E_{\underline{CC}}(\mathbf{k})} \\ &\equiv \frac{m}{\hbar^2} \frac{\partial^2 E_{\underline{CC}}(\mathbf{k})}{\partial k_\alpha^2}. \end{aligned} \quad (\text{A6})$$

It is interesting also to note that for the case considered in Section 3 ($\varepsilon_{\underline{c}}(\mathbf{k}) = -\varepsilon_c(\mathbf{k})$, $\Delta(\mathbf{k}) = \Delta_2^0$), the $\alpha = a$ vertices read as

$$\begin{aligned} \gamma_{aa}^{\underline{CC},CC}(\mathbf{k}; 2) &= \mp \cos \varphi(\mathbf{k}) \gamma_{aa}^{cc}(\mathbf{k}; 2), \\ J_a^{\underline{CC},CC}(\mathbf{k}) &= \mp \cos \varphi(\mathbf{k}) J_a^{cc}(\mathbf{k}), \\ J_a^{\underline{CC}}(\mathbf{k}) &= \sin \varphi(\mathbf{k}) J_a^{cc}(\mathbf{k}), \end{aligned} \quad (\text{A7})$$

where $\gamma_{aa}^{cc}(\mathbf{k}; 2) = \gamma_{aa}^{cc}(\mathbf{k}) = (m/\hbar^2) \partial^2 \varepsilon_c(\mathbf{k})/\partial k_a^2$ and $J_a^{cc}(\mathbf{k}) = (e/\hbar) \partial \varepsilon_c(\mathbf{k})/\partial k_a$ are the vertices of the $\Delta_2^0 = 0$ model.

-
- [1] K. Bechgaard, C.S. Jacobsen, K. Mortensen, H.J. Pedersen, N. Thorup, *Solid State Commun.* 33 (1980) 1119.
- [2] C.S. Jacobsen, D.B. Tanner, K. Bechgaard, *Phys. Rev. Lett.* 46 (1981) 1142; *Phys. Rev. B* 28 (1983) 7019.
- [3] M. Dressel, A. Schwartz, G. Grüner, L. Degiorgi, *Phys. Rev. Lett.* 77 (1996) 398.
- [4] A. Schwartz, M. Dressel, G. Grüner, V. Vescoli, L. Degiorgi, T. Giamarchi, *Phys. Rev. B* 58 (1998) 1261.
- [5] V. Vescoli, L. Degiorgi, W. Hendersson, G. Grüner, K.P. Starkey, L.K. Montgomery, *Science* 281 (1998) 1181.
- [6] L. Degiorgi, M. Dressel, A. Schwartz, B. Alavi, G. Grüner, *Phys. Rev. Lett.* 76 (1996) 3838.
- [7] L. Degiorgi, B. Alavi, G. Mihály, G. Grüner, *Phys. Rev. B* 44 (1991) 7808.
- [8] S. Uchida, T. Ido, H. Takagi, T. Arima, Y. Tokura, S. Tajima, *Phys. Rev. B* 43 (1991) 7942.
- [9] S. Lupi, P. Calvani, M. Capizzi, P. Roy, *Phys. Rev. B* 62 (2000) 12 418.
- [10] F. Venturini, Q.-M. Zhang, R. Hackl, A. Lucarelli, S. Lupi, M. Ortolani, P. Calvani, N. Kikugawa, T. Fujita, *Phys. Rev. B* 66 (2002) 060502.
- [11] D. Pedron, R. Bozio, M. Meneghetti, C. Pecile, *Phys. Rev. B* 49 (1994) 10 893.
- [12] P.A. Lee, T.M. Rice, P.W. Anderson, *Solid State Commun.* 14 (1974) 703.
- [13] G. Grüner, *Density Waves in Solids*, Addison-Wesley, New York, 1994, and references therein.
- [14] A. Virosztek, K. Maki, *Phys. Rev. B* 37 (1988) 2028; *Phys. Rev. B* 39 (1989) 616.
- [15] T. Giamarchi, *Physica B* 230 (1997) 975; *Phys. Rev. B* 44 (1991) 2904.
- [16] V.J. Emery, S.A. Kivelson, *Phys. Rev. Lett.* 71 (1993) 3701.
- [17] J. Favand, F. Mila, *Phys. Rev. B* 54 (1996) 10 425.
- [18] Y. Suzumura, M. Tsuchiizu, G. Grüner, *Phys. Rev. B* 57 (1998) 15 040.
- [19] I. Kupčić, *Physica B* 322 (2002) 154.
- [20] C.A. Perroni, V. Cataudella, G. De Filippis, G. Iadonisi, V. Marigliano Ramaglia, F. Ventriglia, *Phys. Rev. B* 67 (2003) 094302.
- [21] I. Kupčić, unpublished.
- [22] J. Voit, *Rep. Prog. Phys.* 57 (1995) 977.
- [23] P.M. Chaikin, *J. Phys. I France* 6 (1996) 1875.
- [24] A.M. Gabovich, A.I. Voitenko, J.F. Annett, M. Ausloss, *Supercond. Sci. Technol* 14 (2001) R1, and refereces therein.
- [25] W. Götze, P. Wölfle, *Phys. Rev. B* 6 (1972) 1226.
- [26] D. Forster, *Hydrodynamic Fluctuations, Broken Symmetry and Correlation Functions*, W.A. Benjamin, London, 1975.
- [27] G. Jackeli, N.M. Plakida, *Phys. Rev. B* 60 (1999) 5266.
- [28] V.J. Emery, R. Bruinsma, S. Barišić, *Phys. Rev. Lett.* 48 (1982) 1039, and references therein.
- [29] N. Thorup, G. Rindorf, H. Soling, K. Bechgaard, *Acta Cryst. B* 37 (1981) 1236.
- [30] Notice that the case $\mathbf{Q} \rightarrow \mathbf{Q}_1 \approx 4\mathbf{k}_F$, $\Delta(\mathbf{k}) \rightarrow \Delta_1(\mathbf{k})$ describes the bond-energy dimerization discussed in the previous section.
- [31] J.M. Ziman, *Electrons and Phonons*, Oxford University Press, London, 1972.
- [32] It is easily seen that for $2\Delta^0/E_g \ll 1$ it is even allowed to omit the first contribution in Eq. (14) and treat H'_0 on an equal footing with H'_1 . In this limiting case, $J_{\alpha}^{CC}(\mathbf{k}) = 0$ and $H' \approx H'_0 + H'_1$.
- [33] G.D. Mahan, *Many-Particle Physics*, Plenum Press, New York, 1990.
- [34] Notice that the approximation $n_{\text{intra},\alpha}^{\text{eff}} \approx n$ is appropriate when the carriers behave as ordinary electrons/holes, including the tight-binding electron/hole systems below quarter-filling; here n is the electron/hole concentration.
- [35] It is important also to notice that for $\delta \approx 1$ and $\hbar\Gamma_{\text{inter}} > \Delta^0$ the distribution function $f_{\underline{C}}(\mathbf{k})$ becomes relevant as well. In order to ensure the conductivity sum rule for this case, the summation \sum_L must be included in the expressions (17), (21) and (29). The complete form of the related optical conductivity is given in Sec. 3.2.
- [36] D. Pines, P. Nozières, *The Theory of Quantum Liquids I*, Addison-Wesley, New York, 1989.
- [37] I. Kupčić, *Physica C* 391 (2003) 251.
- [38] Notice the maxima in $n_{\text{total},b'}^{\text{eff}}$ which separate the doping range corresponding to the open Fermi surface from the ones representing the closed Fermi surfaces.
- [39] D. Jérôme, H.J. Schulz, *Adv. Phys.* 31 (1982) 229.
- [40] S. Doniach, E.H. Sondheimer, *Green's Functions for Solid State Physicists*, W.A. Benjamin, London, 1974.
- [41] A.A. Abrikosov, L.P. Gorkov, I.E. Dzyaloshinski, *Methods of Quantum Field Theory in Statistical Physics*, Dover Publications, New York, 1975.